Field trial of a reinforced landfill cover system: performance and failure

Giampaolo Cortellazzo [a], Luis E. Russo [b], Stefano Busana [c], Laura Carbone [d], Marco Favaretti [a, *], Hartmut Hangen [d]

[a] *Dept. ICEA, University of Padova, Italy*
[b] *Huesker Srl, Italy*
[c] *Freelance Engineer, Italy*
[d] *Huesker Synthetic GmbH, Germany*

ARTICLE INFO

ABSTRACT

The geotechnical stability of an inclined multilayer capping depends on the shear strength available along the various interfaces. If the slope is very steep an additional reinforcing geosynthetic may be used to obtain a safer condition. Full-scale field trials can provide better resolution data on the reinforcement behaviour than conventional calculation methods based only on laboratory tests. The paper deals with a field trial carried out on multilayer capping, reinforced with a geogrid, in an Italian landfill. The geogrid behaviour was monitored for a month using displacement sensors and pressure cells located along the slope and in the anchor trench. Subsequently, the cover system was led to collapse by cutting the reinforcement and an analysis of the reinforcement behaviour and its relevance in the system stability were studied. This paper discusses in detail the setup of the field trial and the experimental data recorded during installation, monitoring, and failure phases of the system. The deformation behaviour of the geogrid during the entire test was recorded and analysed. The resulting data highlight the effects of the construction process on the geogrid behaviour including the contribution of geogrid creep characteristics until the failure.

1. Introduction

The adoption of multilayer barrier systems, composed by soil and geosynthetic products, has become common place in construction technology used in municipal solid waste landfills. When multilayer systems are laid on slopes, the weight of the cover soil induces a driving force that tends to move the system downward. In order to counteract this force, it is essential: 1) to consider the stress-strain relations of each component of the system (Jones and Dixon, 2003) and 2) to estimate the frictional forces capable of developing along the interface surfaces between two geosynthetics and between geosynthetics and soil (Carbone et al., 2013, 2015). When the cover surface is at a steep angle, an additional reinforcement geogrid, usually anchored at the top of the slope or along intermediate benches, may be necessary to obtain the required factor of safety against sliding.

Many methods are available to perform slope stability analysis of the cover system whether they are closed-form analytical using limit equilibrium methods (Giroud and Beech, 1989; Thiel, 1998; Koerner and Soong, 1998; Zornberg, 2005), or numerical methods (Fowmes et al., 2008; Tano et al., 2017; Kavazanjian et al., 2018; Yu and Rowe,

2018). A further analytical method that allows to estimate the tensile forces acting in each section of the reinforcing geogrid developed along the entire slope profile was proposed by Russo (2008).

To investigate results obtained from a real scale field test in comparison to state of the art analytical methods, data was collected on the stability of a steep cover system using a field test designed and carried out in 2016 at the municipal solid waste (MSW) "Torretta" landfill in Legnago (Italy). The aim of the research was to analyse the effectiveness of the reinforced cover system and its behaviour at failure. An extensive measurement program was performed during the field test to elucidate the role of geogrid reinforcement in the system stability and its deformation. Furthermore, the testing design allowed analysis of the induced stresses in the geogrid during the construction phase. The data provided additional insight about three characteristic failure mechanisms of this application: sliding, uplift in the trench, and trench tooth collapse. Finally, a previously developed analytical method was used to determine the equilibrium of the system and the tensile forces along the geogrid (Russo, 2008). The analytical results were then compared with those obtained in the real scale field trial. Results from the analytical method were an effective tool in determining the equilibrium system and tensile

* Corresponding author.
E-mail address: marco.favaretti@unipd.it (M. Favaretti).

Note: Low-resolution images were used to create this PDF. The original images will be used in the final composition.

forces; moreover, the field scale test allowed an accurate analysis of failure mechanisms.

2. Background

Common design approaches monitor the cover behaviour during construction and after closure. However, available studies are often related to already collapsed barrier systems (Zamara et al., 2012). Consequently, the performance of these systems is generally back-analysed from large-scale landfill failures, and not from the direct monitoring of operating landfills. This approach has some limitations, as shown by the extensive literature surrounding the failure of the Kettleman Hills Landfill (California). The failure occurred in 1988, along a sliding surface located between one of the interfaces of the barrier system. Mitchell et al. (1990) analysed in laboratory the shear strength characteristics of the different interfaces involved in the failure; and Seed et al. (1990) carried out 2D analyses to determine the cause of the stability failure of the capping. Byrne et al. (1992) re-examined the slope failure causes focusing on the mobilised shear strength at failure compared to the peak and residual shear strengths as subsequently corroborated by studies made by Stark et al. (1996). Chang (2005) further analysed the failure with a 3D limit equilibrium method. However, despite the numerous studies, the real initial conditions remain unknown and the shear strength mobilised in the failure uncertain.

Full-scale geotechnical monitoring research projects allow to investigate landfill barrier behaviour and to predict the acting stresses and strains, so that the assessment of the stability and performance of landfill barriers is reliable throughout the landfill lifetime. Among the limited number of full-scale geotechnical landfill monitoring researches, the following studies may be highlighted:

- three-year in situ monitoring of a HDPE geomembrane liner placed on a 3H:1 V (horizontal: vertical) side slope about 9.2 m long at the Yolo County MSW landfill in Northern California (Yazdani et al., 1995);
- full-scale tests performed on the experimental site at Montreuil sur Barse in France monitoring a slope 1:2 (V/H) about 9.0 m long and with a 0.30 m thick granular cover soil layer (Gourc et al., 1997);
- tests at the Torcy landfill in France with a slope inclination of 3H/1 V, a long term monitoring of the displacement of four different geosynthetic lining systems placed over a 50 m length slope covered with 0.30 m thick soil layer during the next two years after construction (Villard et al., 2000; Feki et al., 2002);
- test at Milegate Extension Landfill (East Yorkshire, UK) (Zamara et al., 2012, 2014).

In particular, the research carried out at Milegate Extension Landfill is one of the most extensive and complete studies of full-scale field tests. The aim of the study was to investigate the mechanical performance of the multi-layered bottom barrier at the side of the landfill consisting of a compacted clay layer overlaid by high density polyethylene geomembrane, geotextile, and sand. Geotechnical instrumentation was used to measure stresses (pressure cells), strains (optical fibres, Demec strain gauges, extensometers), and displacements (extensometers), within the different layers taking into consideration the influence of temperature measured by pressure cell thermistors and air temperature using a thermometer. The measured data have shown the strain changes and redistribution of stresses over time in the geomembrane under constant load due to temperature variations. Moreover, due to the relative displacement between the different interfaces during the soil filling process, the mobilisation of a post-peak strength at the interfaces was detected.

Previous studies highlight that an essential aspect for a correct assessment of stability is the accurate determination of the shear strength between interfaces. Stoltz et al. (2020) summarise the results of several

studies concerning the interface behaviour among geotextiles as assessed through laboratory tests (i.e., shear box test and inclined plane test).

Various factors affect the mechanical behaviour of interfaces concerning geosynthetics, among which include: normal stress (Bacas et al., 2015a; Punetha et al., 2019), moisture content (Ferreira et al., 2015), temperature (Frost and Karademir, 2016), sliding history (Stoltz and Vidal, 2013; Punetha et al., 2019), static or dynamic load conditions (Vieira et al., 2013; Carbone et al., 2015; Punetha et al., 2019) and surface characteristics (smooth or textured) between geotextiles in contact (Stark et al., 1996; Bacas et al., 2015b). Moreover, the value of the interface shear strength depends on the characteristics of the devices, and in particular on the strain rate, used to determine it (Stoltz et al., 2020). In addition, there is still little information about the in situ behaviour of inclined geosynthetic cover systems.

In the landfill Torretta di Legnago, the adopted cover system had a combination of different geosynthetics with unknown interaction between them. For this reason, it was considered essential to make a field trial in real scale to investigate the performance of this particular capping to allow a safe and reliable final design.

3. Landfill characteristics

The "Torretta" landfill is a MSW landfill located in Legnago (Verona - Italy) operating since 1982. It was constructed on the bed of the old Tartaro's river, given the presence of a thick natural clayey barrier. Some enlargements were made afterwards, and areas outside the riverbed were occupied. The landfill looks like a flat hill with perimeter slopes inclined 34° and with lengths of about 11 m. The top surface shows humpbacked shape with average slopes of 3%.

In 2003, having reached their maximum capacity, some cells were closed with a cover system consisting of a layer of compacted clay (thickness = 0.30 m) covered by a topsoil layer (thickness = 0.80 m), in accordance with the regulations of the time.

However, with time, the clay mineral barrier showed some cracks over an area of about 180,000 m^2, which resulted in an increase in leachate production, since about 20% of the rainfall water had infiltrated into the landfill. The increased production incurred a significant rise in the cost of leachate treatment, which the owner was obligated to take charge of for a period of at least 30 years after closure, according to Italian regulations.

In 2015, to overcome this problem, the landfill owner Le.Se. (Legnago Servizi) installed an additional geosynthetic cover system to provide the landfill with a reliable long-term sealing solution. This new final cover system represents an alternative solution not described by the Italian code on landfill cover systems. However, this solution was legally acceptable, as the underlying existing cover complied with the current regulations.

The main target of the secondary top cover was to limit the rainfall infiltration up to a maximum of 2%, implementing a reliable and cost-effective solution. For this purpose, the following geosynthetic barrier system was adopted:

- a 0,6 mm thick PE geomembrane, laid directly on the underlying existing clayey layer (GMB – Fig. 1a),
- a lattice geocomposite drainage layer (GCD – Fig. 1b)
- a planar reinforcing geogrid (GGR – Fig. 1c), used to avoid the sliding of the silty-clayey cover soil, 0.80 m thick, along the slope.

Table 1 summarizes the main properties of the materials used for the field trial from bottom to top (Fig. 2a). The main strength and stiffness properties of the geotextiles are reported in Tables 2–4.

The field test aimed to investigate the behaviour of this specific geosynthetic multilayer system under in situ conditions and during critical phases including installation, operation, and induced failure.
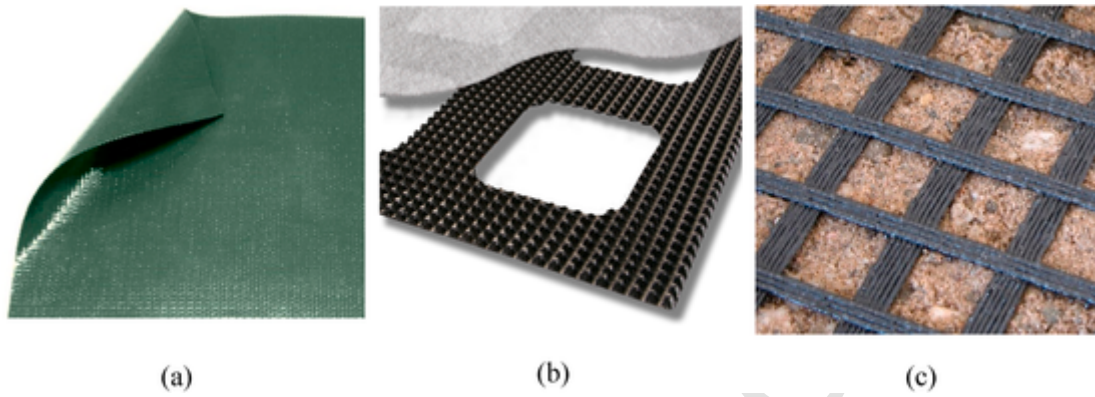
Fig. 1. a) Geomembrane (GMB); b) lattice drainage geocomposite (GCD), laid on the GMB; c) flexible polyethylene (PET) geogrid (GGR).

Table 1
Primary properties of the materials used in Torretta's landfill field trial.

Material	Function	Thickness [mm]	Description
Geomembrane (GMB)	Sealing	0.6	Woven HDPE fabric laminated with LDPE – tarpaulin type
Drainage Geocomposite (GCD)	Drainage/protection	4	Lattice cuspated HDPE drainage core assembled on the cusps with one filtration/protection non-woven geotextile.
Geogrid (GGR)	Reinforcement	1	Flexible PET geogrid with polymeric coating. Nominal tensile strength of 55 kN/m in machine direction
Top soil	Covering/greening	≈800	Silty-clay. Geotechnical parameters: $\varphi' = 26°$; $c' = 9$ kPa and $\gamma = 20$ kN/m^3
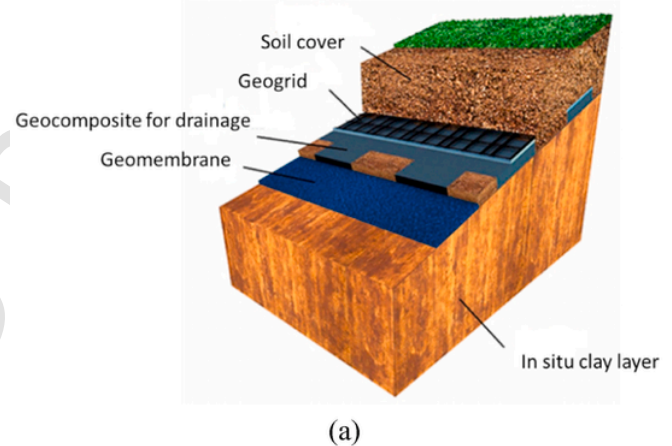
The following responses were analysed during the test:

- geogrid deformation along the slope and in the anchor trench;
- pressure variation from the installation up to the induced collapse, along the anchor zone;
- geogrid interlocking capacity in contact with the geocomposite drain.

4. Field test description: materials and main phases

The tested cover system consisted of a geomembrane, a geocomposite drainage layer, and a high-tensile strength geogrid covered by a minimum of 0.80 m of topsoil.

The primary advantage of geomembrane is the limitation of water infiltration into the waste body due to its sealing function. Consequently, the amount of leachate production is reduced. The geocomposite drainage layer properly drains the infiltrated rainfall water, and the geogrid enhances the stability of the cover soil along the slope against sliding by taking the driven tensile forces and transferring them to the anchor trench at the top.

A planar geogrid was adopted in place of a more expensive tridimensional one commonly utilized in Italy for veneer stability. The inclusion of a lattice geocomposite drainage layer, characterised by square depressions on its surface (Figs. 1b and 2a), enhances the interlocking between the soil and the geogrid. The geotextile covers completely the drainage core and the open squares in it; furthermore, the geotextile is firmly glued to the top of the core cusps.

The schematic cross section of the field trial is shown in Fig. 2b. The field trial was carried out in the steepest landfill section with a slope of 34°. The slope length was equal to 11 m and the geosynthetics had a total width of 3.3 m. The horizontal anchor length of the GGR in the trench was 6.5 m, while the horizontal length of GMB and the GCD was
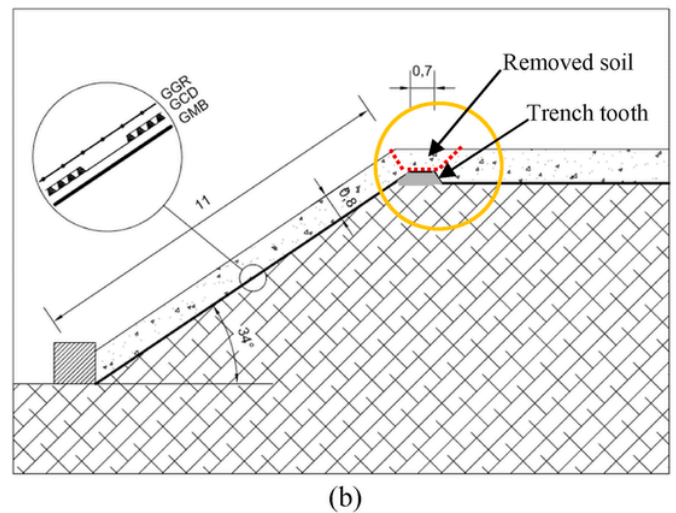
Fig. 2. (a) Multilayer cover system used in the field test; (b) schematic cross section of the Torretta landfill field trial (units [m]).

1.80 m, terminating just before the displacement transducer W5, for experimental purposes. At the toe of the slope, four removable blocks were installed to simulate the passive earth pressure during installation and operational phase (Fig. 3a and b). The blocks were carefully removed to facilitate the failure during the induced collapse phase. At about 0.70 m from the top of the slope, the geogrid was also fixed between two rectangular steel bars to transmit the load of the entire slope to the remaining geogrid strip during the failure phase (Fig. 3a).

The final layout of the field test site is shown in Fig. 3b.

Table 2
Properties of the HDPE geomembrane (GMB).

Property	Value
Thickness (mm)	0.60
Unit weight (kg/m^2)	0.380
Nominal tensile strength at break - machine direction (N/mm)	28
Nominal tensile strength at break - cross machine direction (N/mm)	26
Strain at nominal tensile strength - machine direction (%)	30
Strain at nominal tensile strength - cross-machine direction (%)	24
Tear resistance (N)	964

Table 3
Properties of the (GGR.

Property	Value
Unit weight (kg/m^2)	0.240
Nominal tensile strength at break - machine direction (N/mm)	≥55
Nominal tensile strength at break - cross machine direction (N/mm)	≥25
Strain at nominal tensile strength - machine direction (%)	≤10
Strain at nominal tensile strength - cross-machine direction (%)	≤10

Table 4
Properties of the geocomposite drainage (GCD).

Property	Value
Thickness (mm)	5.8
Mass/unit area (kg/m^2)	0.560
Tensile strength at yield-machine direction (N/mm)	20
Tensile strength at yield cross-machine direction (N/mm)	19
Elongation at yield machine direction (%)	45
Elongation at yield cross-machine direction (%)	45

Fig. 3. Torretta landfill field trial: (a) geosynthetic layers, blocks, sensors, and steel bar; (b) final layout of the field test site.

The following instrumentation was installed to record data during the test (Fig. 4a and b):

- ten GWD 20 type displacement transducers (D.T., acronym Wx) installed on the GGR both in the trench and along the slope for strain measurements along the entire section. The GWD 20 G consists of a flexible insulated foil with an internal resistance track as well as a mounting bracket and a counter plate for strain measurement on geogrids. The foil itself is mounted on a stainless steel carrier. A wiper connected to the plunger loads the foil and works as a voltage divider. The recorded voltage value is proportional to the measured distance, defined by the wiper position. The initial distance between two fixing points was 200 mm. The absolute expansion due to the load was determined with an accuracy of 1%;
  - three one-dimensional pressure cells (P.C., acronym PCx), horizontally located one at the crest of the slope, one at the base of the anchor trench close to the concave vertex and one, at 1.50 m, along the horizontal base of the anchor trench. The pressure cells used electric stress sensors with hydraulic pressure pad and pressure sensor type Glötzl E 40/40 AU. The size of the sensors were 400 mm × 400 mm (PC1 and PC3) and 200 mm × 400 mm (PC2).
- three tensiometers, two along the maximum slope line (at 1/3 and 2/3 of its length) and one at the middle of the anchor trench.
- one static data logger during the one-month monitoring phase and one dynamic data logger during the induced failure phase to store data collected by the D.T.s and the P.C.s.

The field trials were carried out in three main phases:

- installation phase: slope preparation (cleaning and levelling the existing clayey soil) and installation of materials (i.e., geosynthetics and topsoil) and sensors;
- monitoring phase: the data of the displacement transducers and the pressure cells were registered for one month starting from the installation phase;
- failure phase: the system failure was induced slowly by cutting the geogrid on the crest symmetrically, from left and right sides to the centre of geogrid, in steps in order to increase progressively the stress in the remaining strips. In this way, the magnitude of the load supported by the geogrid could be evaluated.

After shaping the trench section, the first step was to locate three pressure cells (PC1, PC2 and PC3) along the trench profile where the highest variation of pressure transmitted to the ground by the geogrid was expected (Fig. 4b). The aim was to measure, during the failure phase, the increase of pressure transmitted by the geogrid to the crest (PC1) and the pressure decrease in the trench internal concave vertex caused by the geogrid uplift effect (PC2), both due to the progressive increase of tensile forces in the remaining strip of uncut geogrid. Pressure cell PC3 was placed in a more stable zone as reference. Afterwards, the geomembrane was installed on the clay layer of the previously existing capping. The geocomposite drainage layer was placed on the geomembrane and the flexible geogrid, with the load distribution steel bars, was installed on the geocomposite drain.

The geogrid was equipped with ten displacement transducers, placed along the central longitudinal axis, connected to a data logger and to a data acquisition system that recorded the geogrid displacements during the different phases of the field trial. This allowed accurate measurements of the mobilised strain and the consequent assessment of the activated stresses of the geogrid along the slope and in the anchor trench. Fig. 4a and b shows the position of the sensors and the steel bars.
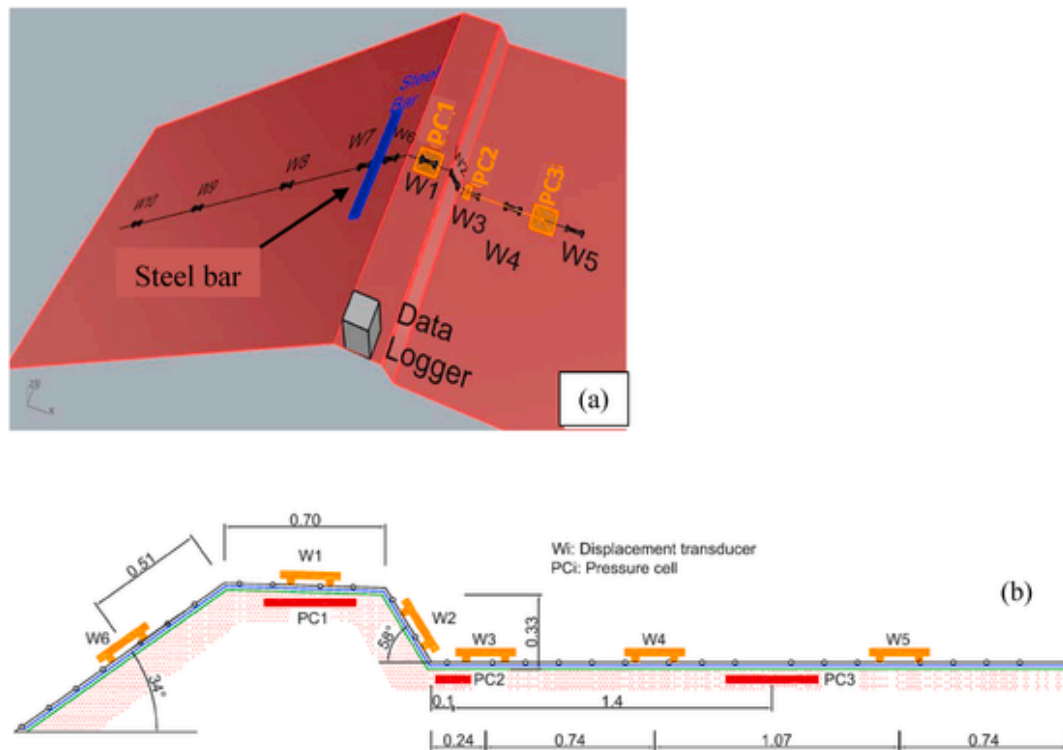
Fig. 4. (a) Location of the displacement transducers and pressure cells; (b) layout of the devices placed along the anchor trench (units [m]).

Afterwards, the anchor trench and the slope crest were filled with soil to fix the geosynthetics. The soil was placed along the slope starting from the top towards the bottom and ending from the toe of the slope, reaching an average cover soil thickness of about 0.80 m. Therefore, a top-down placement of the soil was used to assure the activation of tensile forces in the geogrid, in particular in the trench zone, with the aim of achieving the most adverse design situation. The soil was distributed by the excavator and it was compacted using the bucket.

Two specimens of the cover soil were collected for geotechnical laboratory analysis, and then the slope was covered with a geotextile to protect it from erosion.

The monitoring phase of the cover system lasted 32 days. Topographic measurements were performed on 15 points during the preparation of the section and in the final stage, to get a precise profile of the slope and the cover layer, in order to monitoring eventual changes in time. No significant displacements were observed, since all of them were below 10 mm, that is, within the order of the measurement errors.

After 32 days, the collapse of the cover system was induced.

At the beginning of the failure phase, three tensiometers were temporarily installed at a depth of 0.60 m on the slope and on the anchor trench to measure the suction in the topsoil layer. The measured values had the same order of magnitude: the tensiometer close to the foot of the slope measured −20 cbar, the second one at the middle of the slope −10 cbar, and that on the trench −20 cbar.

Subsequently, the blocks at the slope toe, the protective geotextile, and the cover soil on the top of the anchor trench tooth were slowly removed. This last removal required digging of a trench over the entire width (3.30 m) until the geogrid and the W1 transducer were carefully discovered (Fig. 2b). The geogrid was simultaneously and symmetrically cut from both sides along two lines in the transversal direction, starting from the external longitudinal fibres. After each cut, the operators waited about 5 min before doing the next one and, in any case, up to the complete strain stabilisation verified through the monitoring devices. This operation was done till a width of 0.68 m of uncutted GGR was obtained, with the displacement transducer (W1) in the middle. As previously stated, the aim of this operation was to reduce the resisting section of the GGR, holding the load transferred by the cover soil, along the whole slope and increase the tensile forces to induce the collapse.

During the cutting, the slope remained stable, but a slow progressive separation between the edges of the cut fibres was observed highlighting a slow downward displacement. It was observed that the threads of the geogrid were subjected to high tensile stress. However, since no incipient failure was observed, the lateral soil along both sides of the slope section and some material at the foot were removed to eliminate their contribution to stability and to ensure that the whole weight of the soil along the slope was sustained only by the geogrid and the friction between the GMB and GCD (Fig. 5a).

The slope failed 9 h later under dry ambient. The critical slip surface of the system occurred along the interface between the geocomposite drainage layer and the geomembrane, as expected. During the controlled failure process, the soil, the geogrid, and the geocomposite drainage layer located on the slope behaved as a rigid body (Fig. 5b).

The 0.68 m wide remaining geogrid held the load transferred by the whole slope for an elapse of 9 h with the help of the shear strength developed along the critical sliding surface. The geogrid was subjected to a exponential increase of tensile force that caused an acceleration of the creep phenomenon.

Moreover, a significant lifting of the GGR was observed near the crest in the concave corner of the trench due to the tensile forces developed in the geogrid. A horizontal crack was observed at the base of the trench tooth denoting the generation of high shear stresses during the final phase of the test.

5. Soil and interface properties

Grain size distribution (ASTM D6913/D6913M), liquid limit, plastic limit (ASTM D4318), and consolidated undrained triaxial (CIU - ASTM D4767) tests were carried out on the cover soil specimens. They were collected in the field test site manually driving a thin-walled sampler perpendicularly to the slope surface up to a depth of 0.80 m from the ground level.

Fig. 5. (a) Slope after the removal of the soil at both sides; (b) failed slope and broken fibres (view from the top).

The two specimens resulted to be of silty-clayey soil (ML 1st sample-CL 2nd sample) with a unit weight of 20 kN/m^3. The index properties are Liquid limit w_L = 36–41%, Plastic limit w_p = 23–27% and Plasticity index Ip = 13–14%.

Three couples of triaxial tests were performed using a back-pressure of 400 kPa and confining pressures of 425, 450, and 500 kPa. The calculated soil strength parameters referred to high strain levels ($\approx$ 15%) were c' = 9.0 kPa and φ' = 26°. These tests were carried out to determine the minimum soil resistance without considering unsaturated behaviour, since the achievement of complete saturation of the cover soil might occur in presence of intense rainfalls and cracks in the cover soil. With this hypothesis the overall stability of the cover soil was preliminarly calculated and the resulting global safety factor was about 1.25.

The peak friction angle at the interface between the GM and the GCD was between 20.5° and 20.9°, upon the assumption of zero adhesion; it was determined fixing the GM on a rigid perfectly planar support surface, placing the GCD and 0.20 m of sand over it and tilting the support slowly (EN ISO 12957–2:2005, 2015). An overall pressure of 12 kPa was applied.

6. Analysis of the experimental data

6.1. Installation and monitoring phases

The measured values of vertical normal pressures at the end of the installation phase are reported in Table 5. The highest value was measured by PC3, where the soil layer was thicker (1.10 m) and likely more compacted due to movement of the excavator. These values were consistent with soil thickness and unit soil weight therefore the reliability of the measured data was substantiated.

During the construction phase, the displacement transducers measured geogrid elongations up to +2.7%. Only the transducer W10, close to the slope toe, registered a compression value of −0.4% (Fig. 6). After the month of monitoring, the sensors W1, W6 and W7 registered a significant increase of strain (in the order of 0.2%). This variation developed over a longitudinal length of 1.8 m (0.75 m on the crest and 1.05 m along the upper part of the slope) and may have been caused by creep strain which was also indicated by the horizontal cracks at the top of the slope. The other displacement transducers registered only small variations, that is, in the order of 0.04%.

Table 5
Measured vertical pressures at the end of installation phase.

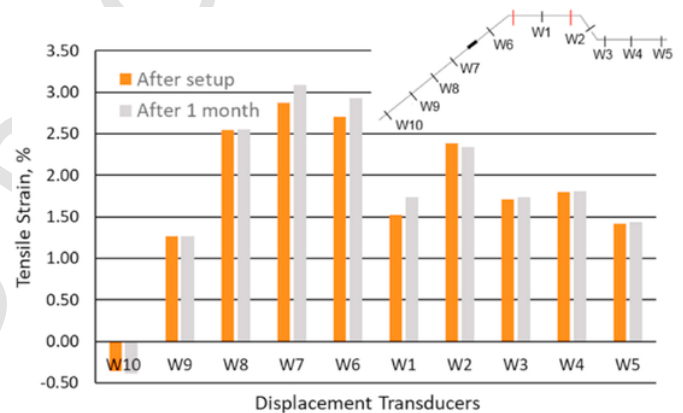| Pressure Cell	Soil thickness [m]	Pressure [kPa]
PC1	0.72	18.7
PC2	0.93	18.6
PC3	1.10	26.5

Fig. 6. Geogrid tensile strain recorded by the displacement transducers after setup and after one-month monitoring phase along the slope and in the anchor trench.

The measured data suggested that the installation sequence of the top soil influenced the initial strain state of the geogrid. Initially, the GGR was fixed by soil in the anchor trench without tensile forces being transferred by the soil weight on the slope. After installation of the soil cover along the slope from the top, activated strains were observed in the GGR.

Measured negative values at W10 were likely to indicate the compression of the geogrid due to the soil cover placement method, initially at the top of the slope and lastly from the toe of the slope. The presence of soil accumulation against the box containers and the presence of the box itself prevented, partially or totally, the free deformation of the GGR. Consequently, the elongation of the geogrid due to the tensile strain at the top of the slope induced a small compression effect at the base (Villard et al., 1999).

The strains measured by W1, smaller than those registered by W6 and W2 (Fig. 6), could be explained by the effects of the compactor passages during the installation procedure. In the elapsed time between the slope preparation and the induced failure test, rainfalls were monitored. Only rainfall events of small intensity occurred, and they did not influence either the behaviour or the state of stress of the slope (max. measured rainfall of 9.8 mm/day only for one day).

6.2. Induced failure phase

The cutting phase of the GGR (Section 4) lasted about 1 h, from 16:11 h to 17:12 h. Only after 22 min (16:33 h), the displacements changed with a well-defined trend. Taking into account previously measured strains and the change of the geogrid width, it was estimated that the remaining geogrid strip (0.68 m wide) was subjected approxi-

mately to a load of 70% of its breaking load just after cutting. A progressive relaxation of the whole system was observed following completion of the cutting, regulated mainly by the interface friction angle GMB/GDC and the ground macro irregularities (Fig. 7) along the sliding surface, due to the construction procedure. This caused an increase of the tensile load up to a stress level of about 80% of the geogrid ultimate tensile strength. Affected by the creep behaviour of the GGR, the failure developed over an elapse of about 8 h (from 17:12hr to 1:11hr).

6.2.1. Pressure data analysis

Pressures measured during the failure phase, after the soil removal at the crest, are shown in Fig. 8a. PC3 registered constant pressure with the exception of some initial variations caused by the movements of the excavator in that part of the trench. For the same reason, PC2 clearly shows two pressure peaks at the same time of those registered by PC3. Thereafter, the pressure registered by PC2 decreased linearly with time. In the concave vertex of the anchor trench, a lifting of the geogrid occurred. This lifting generated an uplift of the cover soil layer with subsequent decrease of vertical pressure. Such behaviour was clearly recorded by PC2 placed close to the concave corner, where an increment of tensile stresses on the GGR generated an uplift force.

PC1 registered an initial pressure close to zero, because the overlying soil had been completely removed to cut the geogrid. Subsequently, after the cut, the pressures increased monotonically and linearly. From 23:16, 8 h after the beginning of the cutting phase, the PC1 behaviour changed and the slope of the curve soil pressure versus time became steeper (Fig. 8a). This change occurred concomitantly with the sudden increase of tensile stress acting on the geogrid, which generated a vertical compression on PC1. Fig. 8b shows the direct relation between the increase of strain on W1, along the consequent increase of pressure on PC1. After the failure of the GGR occurred, PC1 and PC2 went back to the initial values.

6.2.2. Behaviour of the geogrid in the anchor trench

The deformations of the geogrid measured by the displacement transducers in the anchor trench are shown in Fig. 9a. W4 and W5, located farther away from the slope, registered values that remained constant throughout the duration of the test. Therefore, there were no effects of the cut of the geogrid in such points. This suggests that the GGR dissipated completely the pull out stresses in the soil in a shorter stretch than the whole anchor length of the geogrid.

Differently, the increase of tensile load acting on the geogrid caused the activation of W1, W2 and W3, with a progressive increase of the measured displacements. W3 started to be activated at 21:00, about 5 h after the start of the cutting phase, probably due to the lifting of the GGR in the internal concave corner of the anchor trench.

For the same reason, the strain at W2 increased from the beginning of the test for 7 h, up to 23:16, and then it became a constant value of approximately 5%. The instrument did not remain fixed in its initial position, but it moved upward along the internal slope of the trench until it reached the surface. Subsequently, the instrument was no more able to follow the change of direction of the strain in the corner and to measure a straight length of the GGR; therefore, the measurements became unreliable.

W1 behaved consistently with what was expected: starting from the cutting phase, the measured strain increased by 1% in 40 min. Subsequently, the strains continued to increase, but more slowly. In the final failure stage (from 23:16), the increase became faster. This behaviour is a typical creep behaviour, comprised of primary (decelerating strain rate), secondary (constant strain rate), and tertiary (accelerating strain rate) phases.

After failure and removal of the covering soil in the trench, an evident horizontal crack at the internal base of the crest tooth across its width was observed. In that zone, the high horizontal stresses caused soil failure. This phenomenon is quite relevant and must always be taken into account in the design (Russo, 2008).

6.2.3. Behaviour of the geogrid along the slope

The steel bars that fixed transversely the geogrid in the upper part of the slope allowed to transfer the weight of the entire block of soil along the slope during the cutting operation to the remaining strip of geogrid. The strains development of the geogrid in time, measured by the displacement transducers along the slope, are shown in Fig. 9b.

At the bottom of the slope, the W10 data highlighted a constant negative strain (compression) of the GGR in that section, even when the passive pressure induced by the box containers at the toe of the slope was removed. Therefore, the bottom section of geogrid did not contribute to stability.

An increase of deformation occurred at W9 starting after 5 h at 21:30, without involving W8 and W7. It was probably due to some localised soil sliding phenomena close to the bottom of the slope, confirmed by the formation of cracks in that section. The greatest strains were registered by W1 and W6, since they were close to the cut section of the geogrid. W6 measured a regular increase of deformation for about 7.5 h (until 23:30), and then the value became constant, due to a breakdown of the displacement transducer. Due to the small distance between W1 and W6 ($\approx$ 1.0 m), the stress and strain variations were quite similar. Taking into account this behaviour, in Fig. 9b, the strains at W6 after 23:30 were extrapolated by maintaining the same ratio between the strains of W6 and W1 measured before the breakdown.

For 7 h up to 23:16, the strain increasing of W1 and W6 was linear; later, the strains of W1 suddenly increased up to failure. Therefore, it seems reasonable to assume a discontinuity in the system behaviour after 23:16. In first part the velocity was 0.58%/hour, whereas during the last 2 h it became 0.955%/hour.

Starting from the beginning, the displacements of the soil block on the slope were calculated. W4 was chosen as the reference point with zero displacement, due to its negligible activity. The overall displacements of the soil block below the steel bars were determined by adding the geogrid strain increments measured by W1, W2, W3, and W6, multi-

Fig. 7. Macro irregularities and depressions on the slope surface.
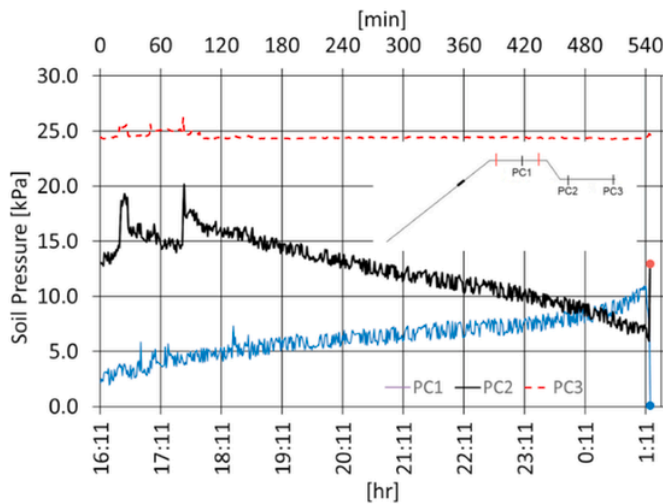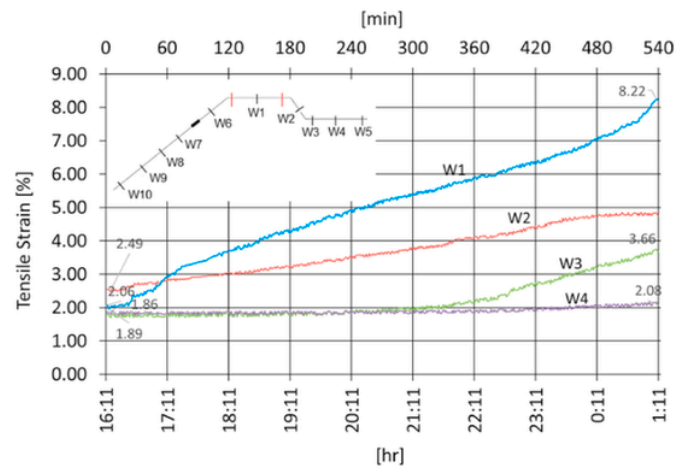
(a)
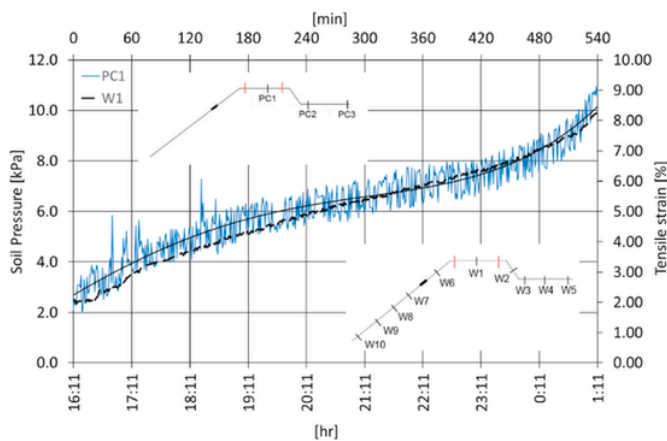
(b)

Fig. 8. (a) Vertical pressures during the induced failure phase; (b) proportionality between the increase of strain in W1 and increase of pressure in PC1, after cutting and until the failure.

(a)

(b)

Fig. 9. Trend of tensile strains recorded by displacement transducers since the cutting until the failure: (a) in the trench; (b) along the slope.

plied by their average tributary length (720 mm, 455 mm, 555.5 mm and 445 mm, respectively) (Fig. 10a). Fig. 10b shows the average velocities of the covering soil block during the induced collapse phase registered every 30 min and each hour. The velocity remained nearly constant, in accordance with the linear increase of strain in the same period. During the last part of the test, the behaviour became clearly non-linear.
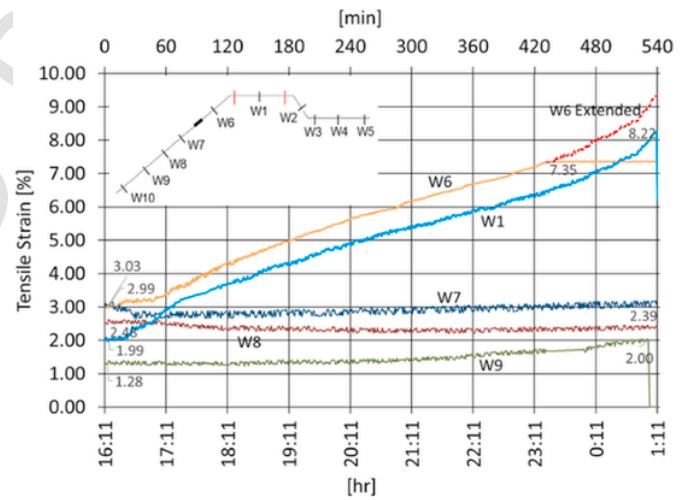
The calculated data confirmed again two different behaviours:

- the first one, lasting up to 7 h after the start of the cutting phase and characterised by a constant velocity and linear deformation;
- the second one, starting at 23:16 and characterised by sudden changes both in deformation and velocity.

According to visual inspection, the failure occurred close to W1 and not to W6, which should have been more stressed. Indeed, if the development of the deformations in W6 had followed the same trend as W1, the maximum extrapolated strain in W6, equal to 9.36%, would have been very close to the breaking point of the geogrid (average value 9.5% from 5 laboratory tests made on virgin samples). This may be explained as follows: in W6 the load was spread over a wider area and in a greater number of geogrid members buried meshes under the cover soil,

while in W1 few remaining uncovered fibres were subjected to high concentrations of tensile forces.

Fig. 5b shows that some fibres were chopped off in the central part, whereas those in the lateral sides were firstly ravelled and then broken. Probably, from 23:16, 7 h after the beginning, the lateral fibres started to break, increasing the displacement and leading to instability.

7. Slope stability analysis

The slope failure occurred expectedly between the GCD and the geomembrane. As far as it was possible to visually verify, no relative movements at the interface between the geocomposite drainage layer and geogrid, and between the geomembrane and the underlying soil were observed. Moreover, there were no relative displacements between the GCD-GGR and the topsoil, due to the grip effect reached thanks to the interlocking and interaction flexibility of the geogrid (Detert and Lavasan, 2018). Therefore, the slope stability analysis focuses on the sliding interface between the geocomposite and geomembrane. Along this interface, the stability of the slope was provided by friction between the geosynthetics and the tensile force on the GGR.
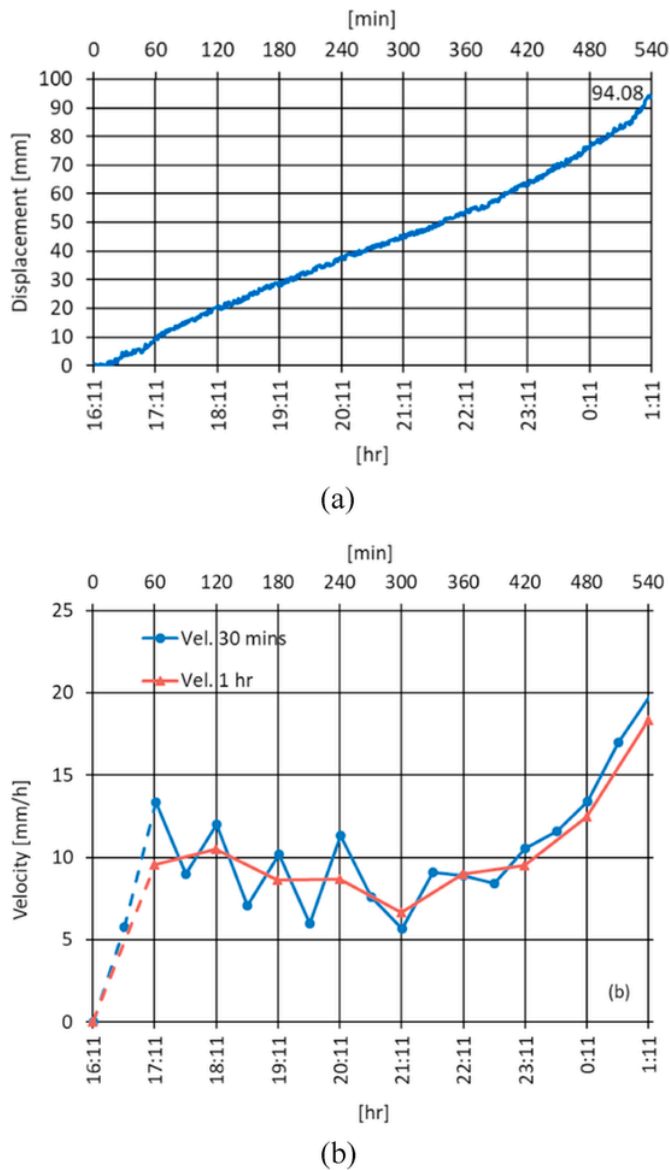
Fig. 10. (a) Soil block displacements; (b) variation of the slope block velocity during the induced collapse phase.

In the following stability evaluation, the minimum mobilised friction angle between the geomembrane and geocomposite drainage layer required for stability is determined.

In a laboratory test for the measurement of geosynthetic interface shear strength using an inclined plane, the slipping phenomenon during the failure phase is described by the general stability equation (Eq. (1)) (Briançon et al., 2011):

$$\frac{W \cdot \sin \beta^* - F(\beta^*)}{W \cdot \cos \beta^*} = \tan \delta(\beta^*) - \frac{\gamma(\beta^*)}{g \cdot \cos \beta^*} \tag{1}$$

where W is the soil block weight, β^* is the slope angle, which increases during the test, $F(\beta^*)$ is the force developed by the reinforcement when resisting to motion, $\gamma(\beta^*)$ is the block component of acceleration parallel to the slope, $\delta(\beta^*)$ is the mobilised variable friction angle at the interface and g is the gravity acceleration.

In the field test, the slope angle remained constant and the ratio between the system acceleration γ and gravity acceleration g was negligible. The slipping phenomenon can be interpreted through a static analysis given the dynamic contribution had a small influence on the determination of $\delta(t)$. The equation may be reduced to:

$$\tan \delta(t) = \frac{W \cdot \sin \beta - F(t)}{W \cdot \cos \beta} \tag{2}$$

where β is the average slope angle, the adhesion is assumed to be zero, and F(t) varies during the failure phase.

The mobilised F(t) varies over time for two reasons:

- changes of strain over time and consequently changes of the mobilised force;
- elasto-visco-plastic load–strain behaviour of the polymer geosynthetic reinforcement materials.

The friction angle (δ) at the interface, is the only unknown parameter and could be determined by imposing the equilibrium of forces.

The stability evaluation was carried out referring to four different times:

- 16:11: just after the removal of the foot blocks and the cut of the geogrid;
- 17:12: soil removal at both lateral sides;
- 23:16: beginning of the nonlinear behaviour of the system;
- 01:11: occurrence of collapse.

As previously stated, strains of W6 from 23:11 up to 01:11, the last 2 h before the failure, were extrapolated from measurements of W1, based on their ratio before the W6 rupture.

After 16:11, the initial resisting section of the geogrid, initially 3.30 m wide for all displacement transducers, became 0.68 m for W1. The effective geogrid width subjected to stress for displacement transducers W6 and W2 was probably closer to 0.68 m than 3.30 m, whereas for W3, W4, W5 it was estimated around 3.30 m.

The forces due to the topsoil weight were calculated using topographic measurements. Different stretches of soil corresponding to each strain gauge, depending on its position along the slope, were taken into account. Therefore, the influence of all cover soil weight along the slope was considered for W6 and only the bottom part for W9.

The tensile force of the geogrid in correspondence of the displacement transducers was determined using the measured strains and calibrated with the specific creep curve of the adopted PET geogrid, since the geosynthetics constituting the materials are characterised by an elasto-visco-plastic behaviour, as observed in several experimental studies. In Fig. 11, the isochronous creep curves of the GGR provided by the manufacturing company are reported. In particular, the stress-strain behaviour related to 1-month creep curve was used to check the displacement registered during one month by the transducers placed on the top of the slope.

The following aspects were determined from the equilibrium analyses:

1) the minimum mobilised friction angle that provided stability over time in correspondence of the displacement transducers along the slope (Fig. 12a);
2) the variation of the average mobilised friction angle from W6 to the bottom and the total displacement of the soil block (Fig. 12b);
3) the variation of the average mobilised friction angle from W6 to the bottom and the corresponding variation of the sliding velocity (Fig. 12c).

For every displacement transducer, Fig. 12a shows the minimum average friction angle at the interface between GM and GCD required to comply with the equilibrium equation (2) between the generic Wi and the bottom.

The calculated friction angle between GM and GCD along the slope (W6–W9) initially ranged around 28°–30° for all displacement transducers and remained practically constant for W7 and W8 during the in-
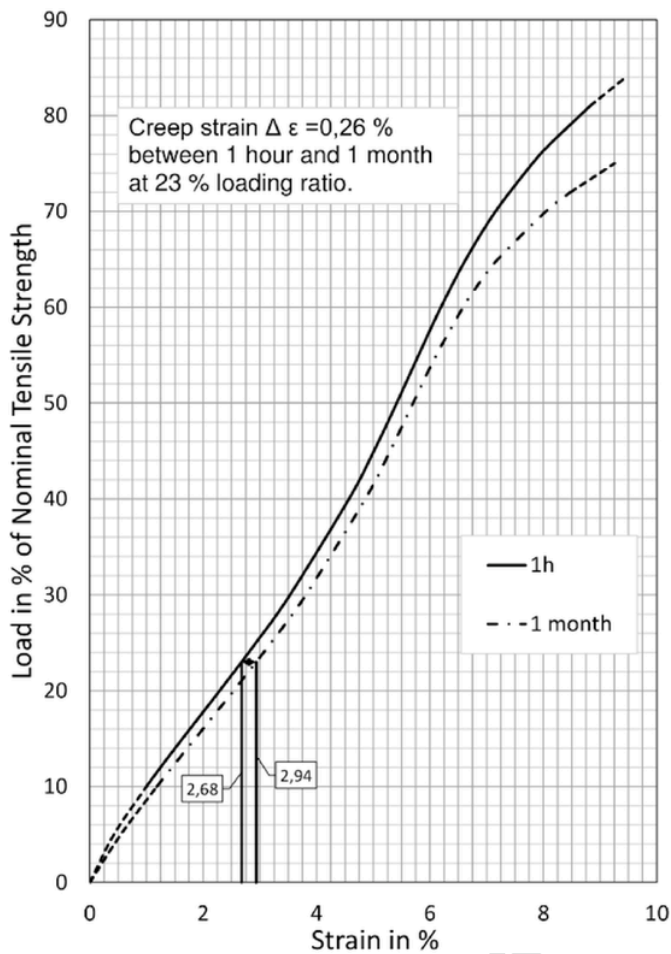
Fig. 11. Geogrid isochronous creep curves at 1 h and one month, highlighting the creep strain variation of transducer W6 during one month and the corresponding percentage of the tensile strength developed in the geogrid.

duced failure phase, whereas it varied considerably for W6, with a peak value and a post-peak shear-softening behaviour. Such values are quite higher than those previously mentioned (20.5° - 20.9°) and obtained by the tests done according EN ISO 12957–2:2005, 2015. The discrepancy may be due to different reasons:

1) the irregularity of the soil surface below the geomembrane which resulted in a macro roughness substantially different compared with the smooth support used in the laboratory test. Fig. 7 clearly shows that the in situ contact surface was not perfectly smooth;
2) the steel bars and bolts used to fix the geogrid, which were pressed against the geomembrane by the top soil and contributed to increase the shear strength of the system;
3) the different shape of the load distribution on the steel bars (uniform load on the whole bars along the downhill side (W7) and only in the central part at the uphill side (W6)) which should have determined its bending.

Fig. 12b presents the variation of the friction angle versus the displacement of the soil block along the slope, showing an increase of the friction angle with small initial displacements up to a peak and then decrease when the displacements increase. Similar behaviour has also been observed in the laboratory (Fowmes et al. (2008), Punetha et al. (2019) and Stoltz et al. (2020)). The tests conducted by these researchers clearly showed a peak shear strength for relatively small displacements. After the peak and since 17:11 up to 23:11, the friction angle decreased linearly while the displacements increased linearly.
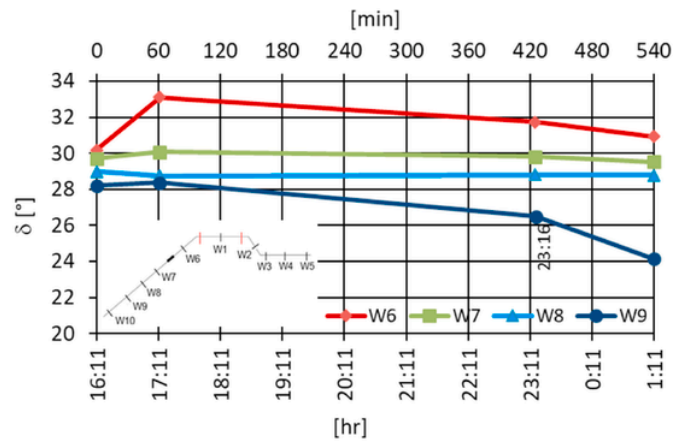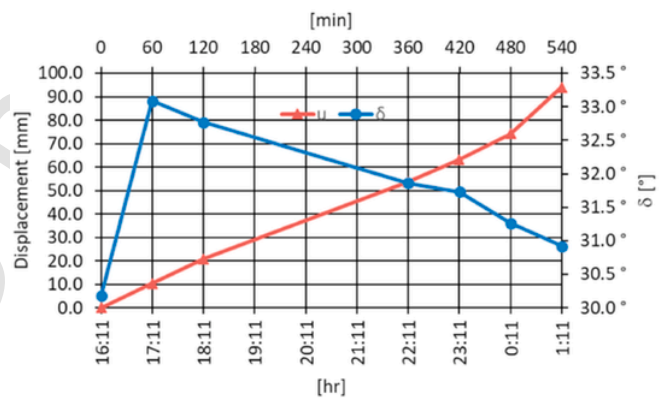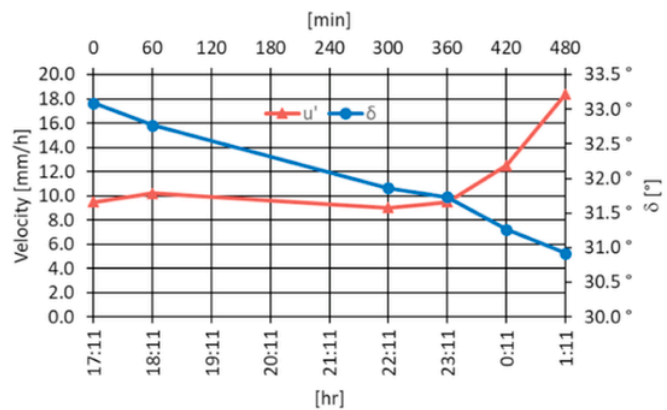
Fig. 12. (a) Average values of friction angles (δ) between GCD and GM, from Wi to the slope foot; (b) block displacement (u) and average values of δ from W6 to the slope foot; (c) block velocity u' and average values of δ from W6 to the slope foot.

Thereafter, there was an acceleration of the displacement with a consequent faster decrease of the mobilised shear strength, until the collapse. The trend of the friction angle versus the sliding velocity at the GMB-GCD interface is reported in Fig. 12c. The magnitude of the interface friction angle depends on the type of geotextiles in contact with each other. In the Torretta's field trial, the critical sliding surface occurred between the smooth geomembrane and the lattice geocomposite drainage layer; therefore, the contact surfaced is mixed, characterised in part by the contact between GMB and the HDPE core of GCD and in

part between the geomembrane and the nonwoven geotextile of GCD (Fig. 1b). Consequently, it is difficult to understand the contribution of each component on the overall interface shear strength; in this field trial, the mobilised friction angle decreases when the speed increases. (Fig. 12c).

8. Mobilised tensile force of the geogrid in the anchor trench

To investigate the difference between theoretical method and the real behaviour on site, a comparison was made between the tensile forces values obtained through measured strains (T_i, i = D.T. number) and those using the analytical method (T_i^*) developed by Russo (2008). For this purpose, the behaviour of the geogrid around the trench tooth was studied, starting from the GGR cutting.

Adopting as starting input the data at W6, the tensile forces determined from measured displacements in the transducers W1, W2 and W3 were compared with those obtained from the calculation. The tensile force in W6, adopted as input data, was obtained with the help of the creep rupture curves shown in Fig. 11. The strain variation under constant load in the elapse of one month was known ($W6_{initial}$ = 2.68% and $W6_{1month}$ = 2.94%), so was obtained the loading ratio equal to 23% of the tensile strength of the geogrid (Fig. 11). From laboratory tensile tests made on the virgin geogrid (according to EN ISO 10319), the average tensile strength was 56.90 kN/m. Therefore, the tensile force calculated through strain data (T_6) on W6 was: $T_6 = 0.23 \times 56.90 = 13.09$ kN/m.

According to Russo (2008), the T_1^* value, before the cutting phase was determined using the expression defined to obtain the tensile forces transmitted through convex corners:

$$T_1^* = \frac{1}{e^{\tan(\varphi_{min})\Delta\alpha}} \cdot T_6 \tag{3}$$

where φ_{min} is the friction angle at the interface between the geomembrane and the geocomposite drainage layer, equal to 21° (the value obtained through the tilting plane test, since the surface was regular and smooth in that section), and $\Delta\alpha$ is the relative angle between the stretches before and after the vertex. From topographic measurements, $\Delta\alpha = 37°$ ($\alpha_{slope} = 35°$ and $\alpha_{crest} = -2°$). Therefore, in this case, the ratio is 0.7804.

$$T_1^* = 0.7804 \cdot T_6 = 10.21 \text{ kN/m} \tag{4}$$

Assuming that such tensile force initially acted on a width of 3.30 m of the geogrid, and then only on the uncut section, 0.68 m wide, the maximum force acting on the geogrid was:

$$T_1^* = 10.21 \cdot \frac{3.30}{0.68} = 49,55 \ kN/m \tag{5}$$

This value is not very different from the geogrid strength obtained by using the creep rupture diagram of the geogrid (Fig. 13, British Board of Agrément BBA, 2019 Hapas certificate 13/H197) considering that the tensile force acting on the geogrid remained constant for the whole duration of the test, 9 h. The percentage of the short-term tensile strength after 9 h (approx. 0,001 year) is 81%, therefore:

$$T_{1,\ ultimate\ 9\ h} = 56.90 \cdot 0.81 = 46.09 \ kN/m \tag{6}$$

The ratio between the calculated T_1^* and the presumed $T_{1,\ ultimate\ 9\ h}$ is about 1.08, a small-amount mismatch.

The increment of tensile force in the remaining strip 0.68 m, wide from a ratio of about 20% to more than 80% of its ultimate tensile strength, accelerated the rupture time due to creep of the geogrid. The analysis shows that the creep phenomenon, inducing a strength reduction, significantly contributed to the failure mechanism, which is con-
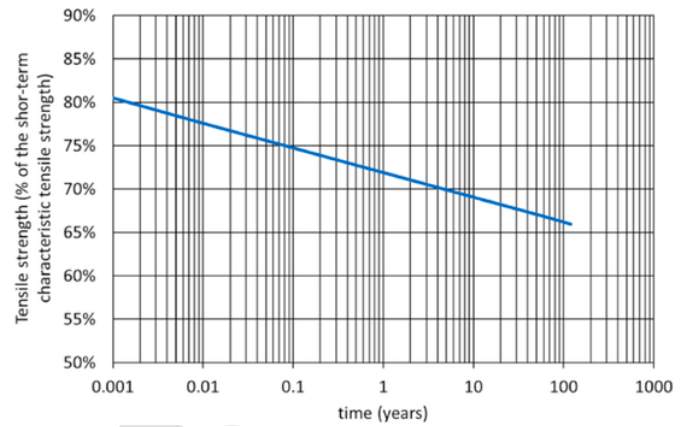

Fig. 13. Creep rupture diagram of the GGR – Regression line for the expectancy of tensile strength at constant stress defined by % of the characteristic short-term strength at 20 °C.

sistent with studies by Di Benedetto et al. (2002), Tatsuoka et al. (2002), and Kongkitkul et al. (2010)..

The validity of equation (3) proposed by Russo (2008) was confirmed by the ratio calculated between T_1^* and T_6, which remained approximately constant from 18:30 to 20:30 (about 0.817) and then increased up to 0.875, probably due to a reduction of the friction coefficient. The approach proposed by Russo (2008) was also used to determine the transfer of force acting on the GGR along whole the crest of the anchor trench taking into account the actual geometry and actions. For the concave corner at the base of the trench tooth, the following expression was used to calculate the force transfer:

$$T_i^* = \frac{\cos\ \alpha_{i-1}}{\cos\ \alpha_i} \cdot T_{i-1} \tag{7}$$

Specifically, it was analysed (starting from W6 as input data) the change of tensile forces in W1, W2, and W3 during the elapse comprised between 19:40 and 22:40 (Table 6), in which the strain development of the system was predominantly linear (Fig. 9a).

The values obtained applying this analytical method were compared with the experimental measurements (Table 6). The deviation between the measured and calculated values was not significant (up to a maximum of 12%) considering the approximations, assumptions, and errors introduced in the procedure in general, which suggest a good correspondence between the analytical results and experimental data.

Table 6
Tensile forces [kN/m] calculated from measured strains (T_i) and with analytical method (T_i^*) starting from T_6, as input data.

Time	T_6	T_1	T_2	T_3	T_1^*	T_2^*	T_3^*	T_1/T_1^* [%]	T_2/T_2^* [%]	T_3/T_3^* [%]
19:40	26.96	22.59	15.58	8.95	21.04	15.53	8.25	7.4	0.3	8.4
20:10	29.22	24.42	16.52	9.39	22.81	16.78	8.75	7.1	−1.6	7.3
20:40	30.77	26.41	17.13	9.45	24.01	18.15	9.07	10.0	−5.6	4.1
21:10	32.65	27.79	17.90	9.56	25.48	19.09	9.48	9.1	−6.3	0.8
21:40	34.31	29.33	18.45	10.05	26.77	20.16	9.78	9.6	−8.5	2.9
22:10	35.80	30.83	19.36	10.33	27.94	21.18	10.26	10.3	−8.6	0.7
22:40	37.01	32.43	20.44	11.21	28.89	22.28	10.83	12.3	−8.3	3.6

9. Conclusions

An appropriate reinforcement geogrid can play a crucial role in the veneer stability of a landfill capping made by a series of geosynthetics layers. This is especially the case if the mobilised interface shear strength between the different layers is not enough to keep the system stable with a suitable degree of safety.

As anti-sliding reinforcement, the geogrid behaviour is commonly analysed by laboratory tests, while there is still little knowledge about its real behaviour under in-situ conditions.

This paper describes a real-scale field trial performed in Torretta di Legnago landfill, where a steep inclined capping made with a geosynthetic multilayer system was induced to collapse. The strain behaviour of the reinforcing geogrid was monitored during the construction and the induced failure phase, through displacement transducers fastened at the geogrid reinforcement.

It was observed that the construction sequence influences the initial stress distribution in the geogrid, and that the geogrid can be differently activated, depending on the covering steps. In this trial test, the soil was placed initially from the top and to end from the bottom, to assure the activation of tensile forces in the geogrid, in particular in the trench zone, and achieve the most adverse design situation.

The pressures cells placed in the anchor trench allowed to understand better the effects of compression and uplift induced by the geogrid, which confirms the expected behaviour.

The collapse happened along the sliding interface between the geomembrane and geocomposite drainage layer, as expected, while the cover soil layer together with the geogrid and geocomposite drainage layer behaved as a rigid body. The adoption of a geogrid with good interaction flexibility (Detert and Lavasan, 2018) facilitate the interlocking between these elements. The mobilised friction angle between GMB and GCD was influenced by the macro irregularities of the underlying surface, which resulted in a higher friction angle value than values determined on a plane surface.

A proper dimensioning of the anchor trench plays an important role in the stability of the entire system; in addition to the required anchor length of the reinforcement, the uplift effect in concave corners and the trench tooth resistance must be verified to prevent anchor failure. In this field trial, the method proposed by Russo (2008) allowed to determine with good accuracy the development of tensile forces along the analysed trench section and could likely be extended for any polygonal sections.

For veneer stability design, it is advisable to determine the long-term tensile strength of the geogrid, through Ultimate Limit State calculation, and to perform Serviceability calculation by taking into account the creep behaviour of the geogrid. This design procedure will allow to keep the long-term strain within allowable values and limit its transfer to the barrier system.

;

References

ASTM D4318 - 17e1 - Standard Test Methods for Liquid Limit, Plastic Limit, and Plasticity Index of Soils.

ASTM D4767 – 11 - Standard Test Method for Consolidated Undrained Triaxial Compression Test for Cohesive Soils1.

ASTM D6913/D6913M - 17 - Standard Test Methods for Particle-Size Distribution (Gradation) of Soils Using Sieve Analysis.

Bacas, B.M., Cañizal, J., Konietzky, H., 2015a. Frictional behaviour of three critical geosynthetic interfaces. Geosynth. Int. 22 (5), 355–365.

Bacas, B.M., Cañizal, J., Konietzky, H., 2015b. Shear strength behavior of geotextile/ geomembrane interfaces. J. Rock Mech. Geotechnical Eng. 7 (6), 345–638.

Briançon, L., Girard, H., Gourc, J.P., 2011. A new procedure for measuring geosynthetic friction with an inclined plane. Geotext. Geomembranes 29 (5), 472–482.

British Board of Agrément BBA, 2019. HAPAS Certificate 13/H197. Product Sheet 3. Huesker Sybthetic GmbH. Fortrac Geosynthetics -Fortrac T and Fortrac R-T Geogrids.

Byrne, R.J., Kendall, J., Brown, S., 1992. In: Seed, R.B., Boulanger, R.W. (Eds.), Cause and Mechanism of Failure Kettleman Hills Landfill B-19, Phase IA. Geotechnical Special Technical Publication No. 31, Stability and Performance of Slopes and Embankments - II, vol. 2. pp. 1188–1215 A.S.C.E.

Carbone, L., Gourc, J.P., Briançon, L., Moraci, N., Carrubba, P., 2013. What value of interface friction to select for geosynthetic liner on landfill slopes? In: Proceeding: Geosynthetic 2013. IFAI, pp. 636–644.

Carbone, L., Gourc, J.P., Carrubba, P., Pavanello, P., Moraci, N., 2015. Dry friction behaviour of a geosynthetic interface using inclined plane and shaking table tests. Geotext. Geomembranes 43, 293–306.

Chang, M., 2005. Three-dimensional stability analysis of the Kettleman Hills landfill slope failure based on observed sliding-block mechanism. Comput. Geotech. 32 (8), 587–599.

Detert, O., Lavasan, A.A., 2018. Relevant properties of geosynthetic reinforcements on the interaction behavior under static and cyclic load conditions. In: Proceedings of the 11th International Conference on Geosynthetics 16-21 September 2018, Seul, Korea.

Di Benedetto, H., Tatsuoka, F., Ishihara, M., 2002. Time-dependent shear deformation characteristics of sand and their constitutive modelling. Soils Found. 42 (2), 1–22.

EN ISO 12957-2:2005, 2015. Geosynthetics - Determination of Friction Characteristics - Part 2: Inclined Plane Test.

EN ISO 10319:2015, 2015. Geosynthetics - Wide-Width Tensile Test.

Feki, N., Villard, P., Gourc, J.P., Chatelet, L., Gisbert, Th, 2002. Comparative long term survey of geosynthetic cap lining systems. In: Proceedings of the 7th International Conference on Geosynthetics, vol. 2, pp. 663–666 Nice, France.

Ferreira, F.B., Vieira, C.S., Lopes, M.L., 2015. Direct shear behaviour of residual soil– geosynthetic interfaces – influence of soil moisture content, soil density and geosynthetic type. Geosynth. Int. 22 (3), 257–272.

Fowmes, G.J., Dixon, N., Jones, D.R.V., 2008. Validation of a numerical modelling technique for multi-layered geosynthetic landfill lining systems. Geotext. Geomembranes 26 (2), 109–121.

Frost, J.D., Karademir, T., 2016. Shear-induced changes in smooth geomembrane surface topography at different ambient temperatures. Geosynth. Int. 23 (2), 113–128.

Giroud, J.P., Beech, J.F., 1989. Stability of soil layers on geosynthetic lining system. In: USA Proc. Geosynth. Conf. pp. 35–46 San Diego.

Gourc, J.P., Berroir, G., Stock, R., Begassa, P., 1997. Assessment of lining systems behaviour on slopes. In: Proceedings of Sardinia 1997, Sixth International Landfill Symposium, vol. 3, pp. 495–506 Cagliari, Italy, CISA.

Jones, D.R.V., Dixon, N., 2003. Stability of Landfill Lining Systems: Literature Review, Environment Agency Research and Development Project P1-385, p. 219 Report 1.

Kavazanjian, Jr., E., Wua, X., Arabb, M., Matasovicc, N., 2018. Development of a numerical model for performance-based design of geosynthetic liner systems. Geotext. Geomembranes 46 (2), 166–182.

Koerner, R.M., Soong, T.Y., 1998. Analysuis and design of veneer cover soil. In: Proceedings of the 6th IGS Conference. IFAI, pp. 1–26.

Kongkitkul, W., Tatsuoka, F., Hirakawa, D., Sugimoto, T., Kawahata, S., Ito, M., 2010. Time histories of tensile force in geogrid arranged in two full-scale high walls. Geosynth. Int. 17 (1), 12–33.

Mitchell, J.K., Seed, R.B., Seed, H.B., 1990. Kettleman Hills waste landfill slope failure. I: liner system properties. J Geotech Eng ASCE 116 (4), 647–668.

Punetha, P., Samanta, M., Mohanty, P., 2019. Evaluation of the dynamic response of geosynthetic interfaces. Int. J. Phys. Model. Geotech. 19 (3), 141–153.

Russo, L., 2008. Design Method for Cover Soil Stability of Lined Multi-Slope/berm Systems Using Continuous Geogrid Reinforcement. The First Pan American Geosynthetics Conference & Exhibition, Cancun, Mexico.

Seed, R.B., Mitchell, J.K., Seed, H.B., 1990. Kettleman Hills waste landfill slope failure. II: stability analyses. J Geotech Eng ASCE 116 (4), 669–690.

Stark, T.D., Williamson, T.A., Eid, H.T., 1996. HDPE geomembrane/geotextile interface shear strength. J. Geotech. Eng. 122 (3), 197–203.

Stoltz, G., Nicaise, S., Veylon, G., Poulain, D., 2020. Determination of geomembrane – protective geotextile friction angle: an insight into the shear rate effect. Geotext. Geomembranes 48, 176–189.

Stoltz, G., Vidal, N., 2013. Alteration of friction characteristics of geosynthetics interfaces following successive slidings. In: Int. Symp. On Design and Practice of Geosynthetic-Reinforced Soil Structures. p. 6p Bologna, Italy.

Tano, B.F.G., Dias, D., Stoltz, G., Touze-Foltz, N., Olivier, F., 2017. Numerical modelling to identify key factors controlling interface behaviour of geosynthetic lining systems. Geosynth. Int. 24 (2), 167–183.

Tatsuoka, F., Ishihara, M., Di Benedetto, H., Kuwano, R., 2002. Time-dependent shear deformation characteristics of geomaterials and their simulation. Soils Found. 42 (2), 103–129.

Thiel, R.S., 1998. Design methodology for a gas pressure relief layer below a geomembrane landfill cover to improve slope stability. Geosynth. Int. 5 (6), 589–617.

Vieira, C.S., Lopes, M.L., Caldeira, L.M., 2013. Sand-geotextile interface characterisation through monotonic and cyclic direct shear tests. Geosynth. Int. 20 (1), 26–38.

Villard, P., Gourc, J.P., Feki, N., 1999. Leachate in landfills: the stability issues. Geotext. Geomembranes 17 (1), 17–32.

Villard, P., Gourc, J.P., Reyes Ramires, R., Thomas, S., Feki, N., 2000. Stability of different inclined cap liner systems- Landfill field trials. EuroGeo 2. In: Proceedings of the 2nd European Geosynthetics Conference, vol. 2, pp. 523–526 Bologna, Italy, 15-18 October 2000.

Yazdani, R., Campbell, J.L., Koerner, G.R., 1995. Long-term in situ strain measurements of

a high density polyethylene geomembrane in a municipal solid waste landfill. In: Geosynthetics '95 Conference Proceedings. pp. 893–906 Nashville, TN.

Yu, Y., Rowe, K., 2018. Modelling deformation and strains induced by waste settlement in a centrifuge test. Can. Geotech. J. 55 (8), 1116–1129.

Zamara, K.A., Dixon, N., Jones, D.R.V., Fowmes, G., 2012. Monitoring of a landfill side slope lining system: instrument selection, installation and performance. Geotext. Geomembranes 35, 1–13.

Zamara, K.A., Dixon, N., Fowmes, G., Russell, D., Jones, V., Zang, B., 2014. Monitoring of a landfill side slope lining system: instrument selection, installation and performance. Geotext. Geomembranes 42, 224–235.

Zornberg, J.G., 2005. Geosynthetic reinforcement in landfill design: US perspectives. In: Zornberg, Gabr, Bowders (Eds.), International Perspectives on Soil Reinforcement Applications. ASCE Geotechnical Special Publication No. 141 Austin, Texas.